Probing Perovskite Carrier Dynamics under Sunlight

Bo-Han Li
Dalian Institute of Chemical Physics, Chinese Academy of Sciences
Huang Li
University of Science and Technology of China
Zhipeng Xuan
Sichuan University
Wen Zeng
Dalian Institute of Chemical Physics, Chinese Academy of Sciences
Jia-Cheng Wang
Dalian Institute of Chemical Physics, Chinese Academy of Sciences
Chuanyao Zhou
Dalian Institute of Chemical Physics, Chinese Academy of Sciences
Xingan Wang
University of Science and Technology of China
Jingquan Zhang
Sichuan University
Zefeng Ren (zfren@dicp.ac.cn)
Dalian Institute of Chemical Physics, Chinese Academy of Sciences
Xueming Yang
Dalian Institute of Chemical Physics

Article

Keywords: perovskite, linear response, ultrafast carrier dynamics

Posted Date: January 11th, 2022

DOI: https://doi.org/10.21203/rs.3.rs-1199100/v1

Probing Perovskite Carrier Dynamics under Sunlight

Bo-Han Li [a, d, †], Huang Li [a, c, †], Zhipeng Xuan [b, †], Wen Zeng [a, d], Jia-Cheng Wang [a, d], Chuanyao Zhou [a], Xingan Wang [c], Jingquan Zhang [b, *], Zefeng Ren [a, *] and Xueming Yang [a, e]

a) State Key Laboratory of Molecular Reaction Dynamics and Dynamics Research Center for Energy and Environmental Materials, Dalian Institute of Chemical Physics, Chinese Academy of Sciences, Dalian 116023, China

b) Institute of Solar Energy Materials and Devices, College of Materials Science and Engineering, Sichuan University, No. 24 South Section 1, Yihuan Road, Chengdu 610065, China

c) Department of Chemical Physics, University of Science and Technology of China, Hefei, 230026, China.

d) University of Chinese Academy of Science, 19 A Yuquan Road, Beijing, 100049, P. R. China

e) Department of Chemistry, Southern University of Science and Technology, 1088 Xueyuan Road, Guangdong, Shenzhen, 518055, China

† These authors contributed equally to this work.

* Authors to whom correspondence should be addressed.

Email addresses: zhangjq@scu.edu.cn; zfren@dicp.ac.cn

Abstract

Understanding the nature of photogenerated carriers and their subsequent dynamics in perovskites is important for the development of related materials and devices. Most ultrafast dynamic measurements on the perovskite materials were conducted under high carrier densities, which likely obscures the genuine dynamics at low carrier densities under solar illumination conditions. In this study, we presented a detailed experimental study of the carrier density-dependent dynamics in hybrid lead iodide perovskites using a highly sensitive transient absorption spectrometer. We found that the carrier lifetime was about a hundred nanosecond in the linear response range, representing sunlight excitation, which was much longer than under high carrier densities. We also elucidated that the fast carrier decay (<1 ps) and the medium decay processes (tens of ps) occurred via the defect state trapping, and we determined its effects on the utilization percentage of photogenerated carriers through quantitative analysis. Furthermore, we obtained the Shockley-Queisser limit that took into account the carrier trapping effect, which directly reflected the material performance.

Keywords: perovskite, linear response, ultrafast carrier dynamics

Solar cell technology is considered one of the best energy shortage solutions for reducing carbon emissions. Over the last decade, perovskite-based solar cells have attracted significant attention and developed rapidly because of its high power conversion efficiency and low fabrication cost, making them one of the most promising solar cell materials.[1, 2] The extraordinary photovoltaic performance of perovskite-based solar cells can be attributed to their strong light absorption,[3] high carrier mobility[4, 5] and long charge diffusion length.[6, 7] Recent progress has been made to improve photovoltaic efficiency in fabrication protocols,[8, 9] chemical compositions[10, 11] and phase stabilization methods.[12, 13] Meanwhile, intense research efforts have also been made to understand these fundamental photophysical mechanisms.[14, 15, 16, 17]

Charge and energy transfer processes occur in solar energy harvesting systems from femtosecond to nanosecond time scales, and understanding these processes is the key to determining the design principle for photovoltaic materials and devices.[17] Ultrafast spectroscopy is a powerful tool that can be used to assess the dynamics of photocarriers in semicondutors.[18] Transient absorption (TA) spectroscopy is the most commonly used method for studying the ultrafast charge and energy transfer processes in perovskites.[18] This technique has been widely used in perovskites to discover the slow hot carrier cooling[7] and reveal the carrier dynamic mechanisms, such as the hot phonon bottleneck,[19] Auger heating,[20] and band filling effects.[21] However, the sensitivity of TA spectrometer is limited; therefore, most reported TA measurements were conducted at much higher carrier densities, such as 10^{17} cm^{-3}, than that under air mass (AM) 1.5G solar illumination conditions.[16] For high-quality methylammonium lead iodide ($MAPbI_3$) films, the calculated carrier density reaches 4×10^{14} cm^{-3} with a monomolecular lifetime of 100 ns under steady-state AM 1.5G conditions in the absence of charge extraction.[16] Carrier-carrier interactions at high carrier densities likely obscures the carrier dynamics at low carrier densities. Hence, to determine the genuine photogenerated carrier dynamics related to solar cells under solar illumination, measurements under low carrier densities are needed.[22]

Here, we report the ultrafast dynamics of photogenerated carriers in hybrid perovskite cesium formamidinium lead iodide ($Cs_{0.1}FA_{0.9}PbI_3$) thin film. It was measured by highly sensitive TA spectrometer, that we recently developed, which enabled us to investigate the carrier dynamics under very low carrier densities. The TA experimental results revealed that carrier dynamics is highly carrier density-dependent with changes of pump intensity. The dynamics in the linear response range showed two fast carrier decays from the trapping process and one slow decay process, which was attributed to the trap-assisted recombination. Additional studies on the thin film with $PbCl_2$ in precursor indicated effective passivation of the trap state density. By quantitative analyzing of the correlation between the TA curve and the carrier capture percentage, we obtained a Shockley-Queisser limit including carrier trapping effects, which quantitatively reflected the performance of solar materials.

Pump Intensity-dependent Carrier Dynamics

The highly sensitive TA spectrometer was developed to study the carrier dynamics of solar energy materials under very low carrier densities.[23] A sensitivity level ($\Delta T/T$) of 10^{-7} was achieved by a novel technique of combining 1 kHz macro-pulse and 200 kHz micro-pulse divided down from a fiber laser with 1 MHz repetition rate and using a balanced detector scheme. The more details of TA spectrometer were described in supplementary information (SI). $Cs_{0.1}FA_{0.9}PbI_3$ thin films was chosen to demonstrate the perovskite carrier dynamics under solar illumination since a partial substitution of Cs^+ for $HC(NH_2)_2^+$ (FA^+)in $FAPbI_3$ perovskite was proved to substantially improve photo- and moisture stability along with photovoltaic performance.[24] $Cs_{0.1}FA_{0.9}PbI_3$ thin films were prepared using a one-step method.(see SI)

First, we conducted ensemble TA spectral measurements of the $Cs_{0.1}FA_{0.9}PbI_3$ thin film under high intensity pumping to obtain the basic TA spectral features. The TA spectra pumped at 50 nJ and 515 nm, as well as 690 nm, are shown in Figures 1 and S7. The carrier density was 2.6×10^{15} cm^{-3}, which corresponded to 1 nJ pump light at 515

nm with a light spot diameter of 3 mm, while 6.7×10^{14} cm^{-3} corresponded to 1 nJ pump light at 690 nm with a diameter of 3.5 mm (see SI). We observed that both TA dynamics were very similar. Immediately after photoexcitation, a ground-state bleaching (GSB, positive change of transmission $\Delta T/T$) band centered at about 790 nm was observed, which was consistent with the band gap obtained from the static absorption spectrum shown in Figure S3. In addition, a photo-induced absorption (PIA, negative $\Delta T/T$) band centered at around 815 nm was observed. The GSB feature was attributed to the band filling, that is the presence of photogenerated band gap carriers blocking the optical absorption of the probe pulse. The PIA was due to the excited state absorption of the hot carriers. After 1 ps, as the hot carriers cooled down the band filling dominated and the PIA disappeared. The GSB signal was longer than 1 ns.

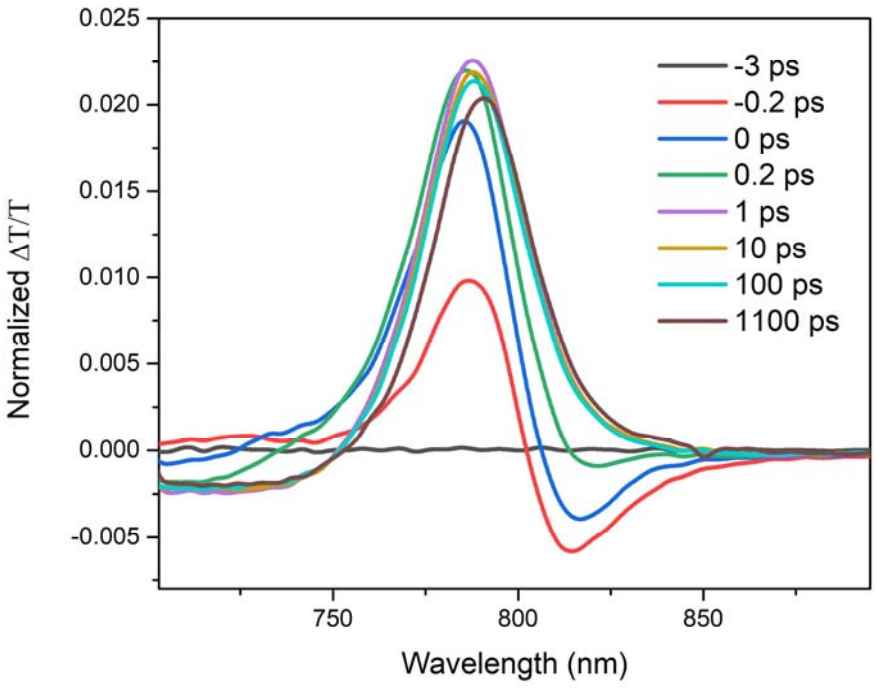

Figure 1. TA spectra. TA spectra of the $Cs_{0.1}FA_{0.9}PbI_3$ thin films plotted at different time delays and transmission change $\Delta T/T$, where the pump energy was 50 nJ per pulse with a light spot diameter of 3 mm and wavelength of 515 nm.

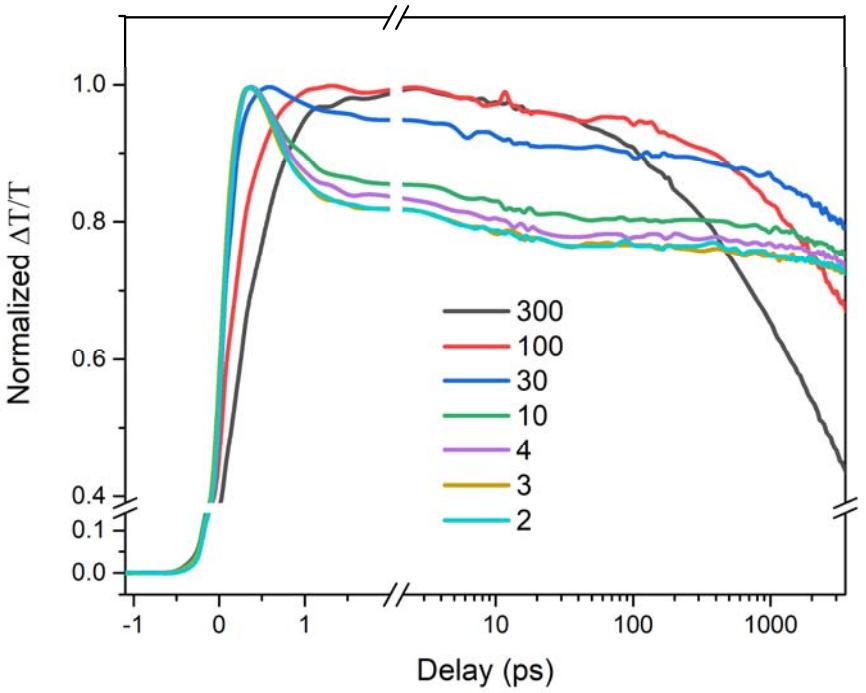

Figure 2. Pump intensity-dependent carrier dynamics. Pump intensity-dependent TA dynamics with a pump wavelength of 515 nm and probe at 790 nm. The normalized changes of transmission $\Delta T/T$ were plotted with different pump energies from 300 to 2 nJ per pulse. Note the shift in time scale from linear to logarithmic, corresponding to the scale break.

To elucidate the carrier recombination mechanism over a range of excitation intensities, the dynamic curve can be modeled by the simple rate equation

$$-\frac{\mathrm{d}n}{\mathrm{d}t} = An + Bn^2 + Cn^3, \quad (1)$$

where n is the photogenerated carrier density and t is the time. The values of the rate coefficients A, B and C for each term differed by many orders of magnitude.[16] Each term in Equation (1) is ascribed to different physical carrier annihilation processes: (1) monomolecular Shockley-Read-Hall recombination, also called trap-assisted recombination, and geminate recombination, which is relatively insignificant for three-dimensional perovskites at room temperature,[25] (2) bimolecular free carrier direct recombination, and (3) three-body Auger recombination. The carrier dynamics is highly dependent on the carrier density. The bimolecular and Auger recombination

mechanisms are most commonly used to elucidate the carrier density decay processes in the reported TA studies, owing to high carrier densities. Figure 2 shows the normalized dynamic traces of the GSB signals at 790 nm for various pump intensities by two orders of magnitude, and some obvious features were clearly observed. First, the rising edge of the GSB signal, which was carrier cooling process, was slower at high pump intensities. This is caused by hot phonon bottleneck effect, which reduces the hot carrier cooling rate when the high density of carriers are excited.[16, 19] (see Figure 3A) Second, at < 1 ps, the quick decay process only appeared at low pump intensities, and the other fast decay process appeared in the tens of picoseconds range. This feature was attributed to the trapping process (see Figure 3B), whose assignment will be discussed in the following section. Third, at a delay range of 100–3500 ps, the decay rate of the GSB signal slowed down with decreasing pump intensity. This was caused by the low bimolecular and Auger decay rates at low carrier densities.[16, 21, 26] Fourth, when the pump energy was below 3 nJ, the normalized TA curves indicated the same dynamics, independent on the pump intensity. Hence, only monomolecular process was observed, without any nonlinear process. Figure S8 shows that the pump energy of the 10 nJ condition at 690 nm reached the linear response range, which was consistent with the carrier density due to the low absorption coefficient at 690 nm. Furthermore, we inferred that under very low pump intensity conditions in the linear response range, the carrier dynamics were the same as that under AM 1.5G. The carrier densities generated by the 3 nJ pump light at 515 nm and 10 nJ at 690 nm were 7.8×10^{15} and 6.7×10^{15} cm^{-3}, respectively, which indicated the upper limit of carrier density in the linear response. This was the first time that the carrier dynamics of three-dimensional perovskites under solar illumination were obtained.

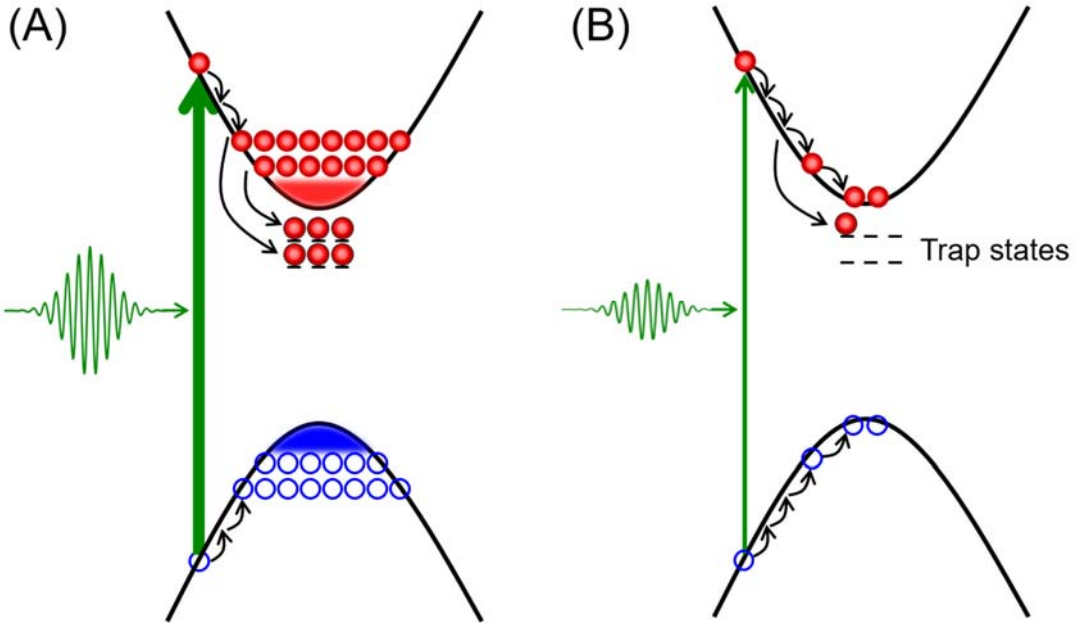

Figure 3. Schematic model of pump intensity-dependent carrier dynamics. (A) High carrier density generated by high-intensity pumping. High carrier density induced hot phonon bottleneck effect and band-gap renormalization. A small percentage of carriers were trapped due to the limited trap state density. (B) Low carrier density generated by low-intensity pumping. A certain percentage of carriers were trapped, proportional to the trap state density. Hole trapping was not indicated in the schematic.

Reports have showed that the band-gap renormalization energy in $FAPbI_3$ under a carrier density of 3.8×10^{16} cm^{-3} was 0.44 meV. [19] In this study, the carrier density was less than 10^{16} cm^{-3} in the linear response range, so the band-gap renormalization can be neglected. Excitons can also be excluded at room temperature due to the small binding energy.[25] Thus, GSB signal decay at 790 nm was only caused by a decline in free carrier density. Recombination has often been considered the main cause for inducing carrier density decay. Both the bimolecular and Auger recombination processes could be excluded as they exhibited strong carrier density dependence and only dominated in high carrier densities.[16] In this study, the pump intensity was sufficiently low that the carrier dynamics reached the linear response range. Hence,

only trap-assisted recombination was possible. This decay process is dependent on the trap cross-section, energy depth, density, and distribution, which were subject to sample processing and handling conditions.[16] However, this process usually lasts tens or even hundreds of nanoseconds.[16] Therefore, we attributed this fast decay process to carries trapping by the defect states, as trapping reduces the densities of the band gap carriers. This has also been widely observed in oxides,[27] perovskite nanocrystals,[14, 28] carbon films[29] and two dimensional materials.[30] And the long decay process was ascribed to trap-assisted recombination.

Carrier Trapping Dynamics in the Linear Response Range

Trap-assisted recombination is considered one of the most detrimental factors to solar cell performance.[2, 25, 31] Carrier trapping is the first step in trap-assisted recombination. In solar cell materials, high-density trap states can induce high trap-assisted recombination rates and low carrier mobility, causing a reduction of open-circuit voltage and loss of short circuit current. In addition, trap states also accelerate the degradation of the perovskite solar cell.[32, 33] Structural defects at interfaces with electron or hole extraction layers, as well as the grain boundaries of perovskite, can induce deep carrier traps,[34, 35, 36] and this has promoted numerous passivation techniques in perovskite solar cells.[37, 38, 39, 40] Due to the importance of traps in perovskite solar cells, many techniques have been developed to probe trap states.[41, 42, 43, 44] Recently, the spatial and energetic distributions of trap states in metal halide perovskite single-crystalline and polycrystalline solar cells were quantitatively measured using the drive-level capacitance profiling (DLCP) method.[34] The researchers found that most of the deep traps were located at the crystal surfaces and interfaces of the polycrystalline films, even after surface passivation. However, these static and kinetic measurements are not enough to comprehensively understand the impact of charge traps on charge transport in perovskite materials and devices on a microscopic level.

The fast decay process in the GSB near the optical gap was only observed under

low carrier densities. However, under high carrier densities, the fast decay was not observed, as the percentage of carriers by trapping was too small because of the limited carrier trap density. (see Figure 3) To quantitatively analyze the carrier dynamics in the linear response range, the TA curve with a pump energy of 3 nJ at 515 nm was fitted by Equation S4, using a function of triple exponential decay convoluted with a time resolution function. The fitting results are shown in Figure 4. A fast decay process was defined as less than 1 ps, a medium rate of decay as about 14.1 ps, and a long decay lifetime was about 70 ns. Limited by the delay line range, the longest decay process was obtained by the approximate extrapolation of a linear decay from Equation S3. The fast decay rate was consistent with the bleaching time scale of the trap states.[14] Both the fast and the medium decay rates were attributed to carrier trapping process, which could be possibility related to the electron and hole traps, respectively.

Although trap bleaching can be directly probed below the optical gap,[14] it is difficult to obtain the beaching signal of all the trapping carriers owing to the wide energetic distributions of the trap states and the normally low trap state density per unit energy.[34] Here, the fast GSB depletion of free carriers was a direct reflections the quantity of trapped carriers as a percentage of the total number of free carriers. Note that this is different from the trap states measured by DLCP. This reported trap state mainly consisted of deep trap states greater than 0.24 eV, which is about 10 times the thermal energy at room temperature.[34] Different trap states have different carrier capture cross sections, which are related to the type of trapped carriers, the energy of the trap states, and temperature.[45] The trap states probed in this work included trap states with broader energetic ranges, as long as they captured carriers. Therefore, the trapping percentage of free carriers derived from the fast reduction of GSB in the linear response range comprehensively revealed the carrier trapping of the working cells under solar

illumination.

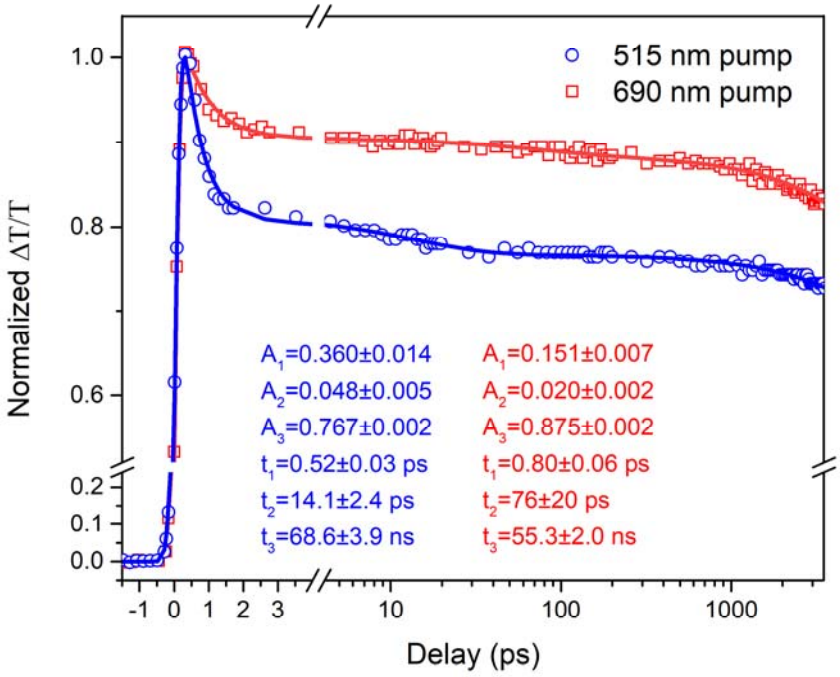

Figure 4. Excitation energy-dependent carrier dynamics. Pump wavelength-dependent TA dynamics in the carrier density linear response range at two pump wavelengths: 515 nm with 3 nJ per pulse (blue) and 690 nm with 10 nJ per pulse (red) and the same probe wavelength at 790 nm. The points indicate the experimental data, whereas the solid lines are fitting results based on Equation S4. A_1, A_2 and A_3 are the initial quantities of three decays, and t_1, t_2 and t_3 are corresponding lifetimes.

To further investigate the characteristics of the trap state in perovskite, additional TA dynamics in the linear response range was measured at a pump wavelength of 690 nm. Figure 3 shows a comparison of the normalzied TA curves at the same probe wavelength of 790 nm with the pump energy of 3 nJ at 515 nm and 10 nJ at 690 nm. The fitting results in Figure 3 shows both the fast decay and the medium rate decay percentages at the pump wavelength of 690 nm were noticeably smaller than at 515 nm. The pump light at 690 nm had a smaller absorption coefficient than at 515 nm; so the carriers created by the 515 nm pump were spatially distributed more concentrated near the surface. The proportion differences between the fast decay with the pump

wavelengths of 515 and 690 nm were mainly due to the different carrier densities near the surface. Because the perovskite defects are mainly concentrated on the surface, carriers near the surface are more easily captured by the defect states. The fast decay and medium decay rate is a little faster at 515 nm excitation than at 690 nm, which was possibly partially due to higher excess energies inducing faster carrier trapping rates, resluting from the interactions with shallow traps.[28] The third longest decay lifetime is shorter at the pump wavelength of 690 nm than at 515 nm. The decay in this time range was due to trap-assisted recombination, along with some carriers diffusion from the crystal interior to the surface, because there were more unoccupied surface defect states at 690 nm excitation.

According to reports on $MAPbI_3$ solar cells,[7] electron transfer to the electron transport layer occurs within 400 ps, while holes transfer to the hole transport layer occurs within 650 ps. In this work, we showed that carrier trapping occured in tens ps, and mostly in less than 1 ps, indicating that the trapped carriers could not be extracted in the perovskite solar cells. Based on the percentage estimation of trapped carriers, we determined that the utilization percentage, η, of photogenerated carriers is only about 65% at 515 nm excitation, and 84% at 690 nm excitation (see SI). A Shockley-Queisser limit, 32.9%, provides a theoretical upper limit efficiency for photovoltaic solar energy conversion by ignoring nonradiative recombination.[46, 47] However, even the best research-cell efficiencies are still much below this limit, owing to the presence of defects.[31] It is often necessary to fabricate a device and measure the cell efficiency to assess the performanace of solar cell matierals, as it is difficult to directly measure how many percentages of free carriers can be utilized under light excitation. Based on above analysis and discussion, we propose to measure TA dynamics at different pump wavelengths, get η at each wavelength, and then obtain η over the solar spectrum. In this work, we based on the assumption that traps distributed at the film surface and interior, and all carriers at surfaces could be captured due to high density of traps at surfaces. Then, according to the absorption depth at different wavelengths, we obtained η as the excitation wavelength in Figure 5 (see SI). Based on the detailed balance limit

for a single junction solar cell,[46] we plotted the transmission, hot carrier cooling and trapping losses (see SI) over the solar spectrum, as well as other losses including emisstion, Carnot and Boltzmann losses.[48] Furthermore, compared to the Shockley-Queisser limit of 30.7% with the band gap wavelength of 790 nm, We calculated the Shockley-Queisser limit as 22.5% inlcuding the loss from the carrier trapping and neglecting the detrapping process.

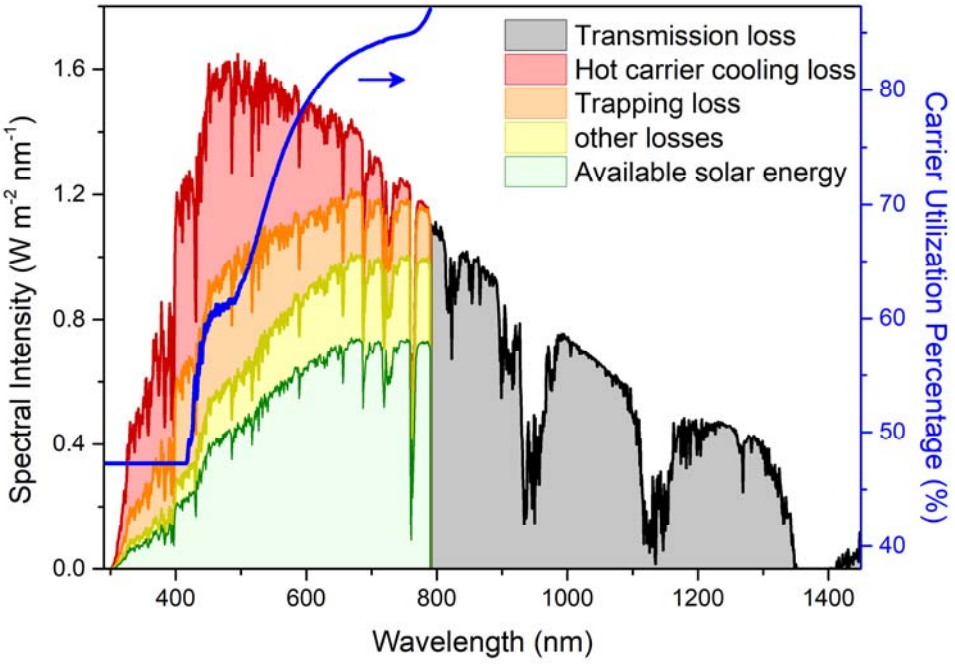

Figure 5. Available solar energy in solar cells. Spectral irradiance of AM 1.5G according to ASTM G173-03 (red and black lines) and the intrinsic losses, such as transmission loss (gray pattern), hot carrier cooling loss (red pattern) and trapping loss (orange pattern), for a single junction solar cell over the solar spectrum based on the detailed balance limit. Other losses (yellow pattern) include emisstion, Carnot and Boltzmann losses.[48] The utilization percentage of the photogenerated carrier, $\eta(\lambda)$, (blue line) as a function of excitation wavelength, where η below 415 nm was set to the same value at 415 nm due to the low signal-to-noise ratio of the absorption coefficient below 415 nm.

Passivation of the surface/interface defects with $PbCl_2$

$PbCl_2$ has been added to precursor solution to form mixed lead iodide perovskites to provide higher solar cell efficiencies,[5, 6] which has been correlated to larger crystal sizes[49] and coherent long-range packing of the crystals in films.[50] It has also been attributed to the passivation of defects and a recudction in the trap state density.[14] Therefore, the passivation effect of $Cs_{0.1}FA_{0.9}PbI_3$ perovskite with the $PbCl_2$ (5%) precursor was investigated by TA dynamics in the linear response range. Figure S9 shows that the GSB peak of the $PbCl_2$-passivated perovskites was 784 nm, a small blue shift from 790 nm. When the pump energy was below 3 nJ, the carrier dynamics was not dependent on the pump intensity (Figure S10). Carrier trapping and trap-assisted recombination were highly dependent on material synthesis.[16] To exclude any randomness, five pristine and five $PbCl_2$ doped samples were tested together, and these curves were consistent, as shown in Figure S11 and Table S1, and Figure 6 shows two typical TA curves for comparison. Compared with the pristine sample, the proportion of the fast decay process noticeably decreased and the medium decay almost disappeared. Furthermore, the carrier lifetime estimated from the third longest decay unambiguously increased, which was consistent with previous reports.[14] This also proved that both of the fast and medium decays were caused by defect trapping. The effects of passivation are generally judged by device performance. In this work, we utilized a direct evaluation method by measuring the ultrafast carrier dynamics. This expedited the feedback process for material synthesis, and further accelerated development of high-performance materials and devices.

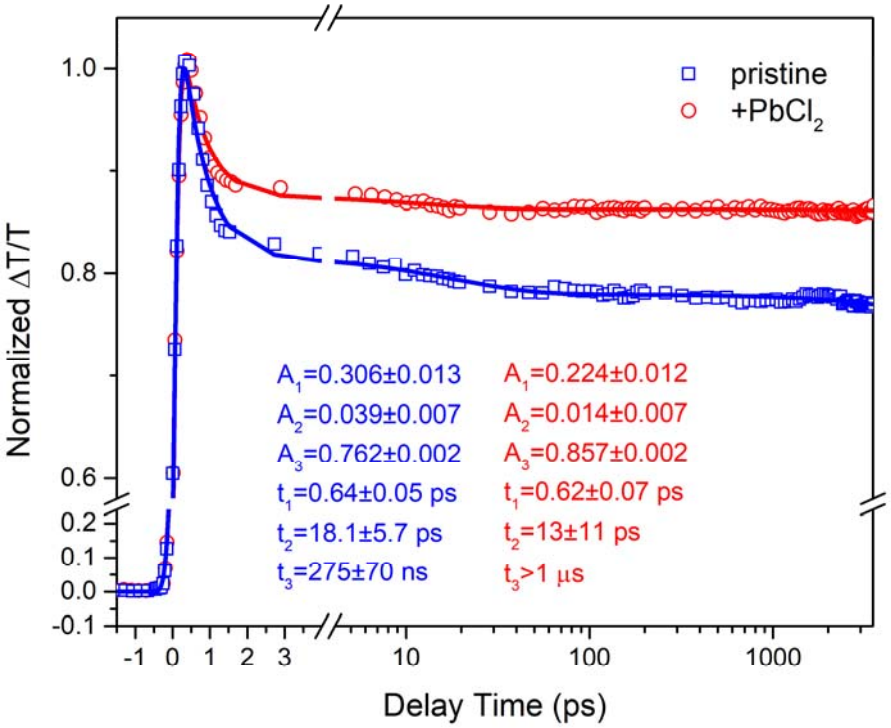

Figure 6. $PbCl_2$ passivation effect. TA curve comparison of carrier dynamics in pristine (blue) and $PbCl_2$-passivated (red) $Cs_{0.1}FA_{0.9}PbI_3$ perovskite thin films, with 515 nm pump and 790 nm and 784 nm probes in the linear response range. The points indicate the experimental data, whereas the solid lines are fitting results based on Equation S4.

In conclusion, we obtained ultrafast carrier dynamics of $Cs_{0.1}FA_{0.9}PbI_3$ perovskite thin films under different carrier densities. At a very low carrier density, the highly sensitive TA spectrometer allowed us to determine the genuine carrier dynamics under sunlight illumnaiton. According to the carrier dynamic curves in the linear response range, we found that the fast trapping process occured in less than 1 ps, and defect-assisted recombination occurred in about a hundred nanosecond. We also extracted the utilization percentages of the photogenerated carriers over the solar spectrum, which were limited by carrier trapping and could be raised by $PbCl_2$ passivation. We obtained an estimation of the Shockley-Queisser limit, accounting for influences from carrier

trapping. These results not only provide a fundamental understanding of the intrinsic photophysical behavior of perovskites under solar illumination conditions, but also provide a suitable method for assessing the performance of perovskite solar cell materials to expedite the process of selecting high-quality materials.

References

1. Kojima, A., Teshima, K., Shirai, Y., Miyasaka, T. Organometal halide perovskites as visible-light sensitizers for photovoltaic cells. *J. Am. Chem. Soc.* 2009, **131**(17)**:** 6050-6051.

2. Kim, J.Y., Lee, J.-W., Jung, H.S., Shin, H., Park, N.-G. High-efficiency perovskite solar cells. *Chem. Rev.* 2020, **120**(15)**:** 7867-7918.

3. Park, N.-G. Perovskite solar cells: an emerging photovoltaic technology. *Mater. Today* 2015, **18**(2)**:** 65-72.

4. Herz, L.M. Charge-carrier mobilities in metal halide perovskites: Fundamental mechanisms and limits. *ACS Energy Lett.* 2017, **2**(7)**:** 1539-1548.

5. Wehrenfennig, C., Eperon, G.E., Johnston, M.B., Snaith, H.J., Herz, L.M. High Charge Carrier Mobilities and Lifetimes in Organolead Trihalide Perovskites. *Adv. Mater.* 2014, **26**(10)**:** 1584-1589.

6. Stranks Samuel, D., Eperon Giles, E., Grancini, G., Menelaou, C., Alcocer Marcelo, J.P., Leijtens, T.*, et al.* Electron-hole diffusion lengths exceeding 1 micrometer in an organometal trihalide perovskite absorber. *Science* 2013, **342**(6156)**:** 341-344.

7. Xing, G., Mathews, N., Sun, S., Lim, S.S., Lam, Y.M., Gratzel, M.*, et al.* Long-range balanced electron- and hole-transport lengths in organic-inorganic $CH_3NH_3PbI_3$. *Science* 2013, **342**(6156)**:** 344-347.

8. Burschka, J., Pellet, N., Moon, S.-J., Humphry-Baker, R., Gao, P., Nazeeruddin, M.K.*, et al.* Sequential deposition as a route to high-performance perovskite-sensitized solar cells. *Nature* 2013, **499**(7458)**:** 316-319.

9. Yang Woon, S., Park, B.-W., Jung Eui, H., Jeon Nam, J., Kim Young, C., Lee Dong, U.*, et al.* Iodide management in formamidinium-lead-halide–based perovskite layers for efficient solar cells. *Science* 2017, **356**(6345)**:** 1376-1379.

10. Jeon, N.J., Noh, J.H., Yang, W.S., Kim, Y.C., Ryu, S., Seo, J.*, et al.* Compositional engineering of perovskite materials for high-performance solar cells. *Nature* 2015, **517**(7535)**:** 476-480.

11. Abdi-Jalebi, M., Andaji-Garmaroudi, Z., Cacovich, S., Stavrakas, C., Philippe, B., Richter, J.M.*, et al.* Maximizing and stabilizing luminescence from halide perovskites with potassium passivation. *Nature* 2018, **555**(7697)**:** 497-501.

12. Saliba, M., Matsui, T., Domanski, K., Seo, J.-Y., Ummadisingu, A., Zakeeruddin Shaik, M.*, et al.* Incorporation of rubidium cations into perovskite solar cells improves photovoltaic performance. *Science* 2016, **354**(6309)**:** 206-209.

13. Min, H., Kim, M., Lee, S.U., Kim, H., Kim, G., Choi, K., *et al.* Efficient, stable solar cells by using inherent bandgap of α-phase formamidinium lead iodide. *Science* 2019, **366**(6466)**:** 749-753.

14. Wu, X., Trinh, M.T., Niesner, D., Zhu, H., Norman, Z., Owen, J.S., *et al.* Trap states in lead iodide perovskites. *J. Am. Chem. Soc.* 2015, **137**(5)**:** 2089-2096.

15. Zhu, H., Miyata, K., Fu, Y., Wang, J., Joshi, P.P., Niesner, D., *et al.* Screening in crystalline liquids protects energetic carriers in hybrid perovskites. *Science* 2016, **353**(6306)**:** 1409-1413.

16. Johnston, M.B., Herz, L.M. Hybrid perovskites for photovoltaics: Charge-carrier recombination, diffusion, and radiative efficiencies. *Acc. Chem. Res.* 2016, **49**(1)**:** 146-154.

17. Shi, J., Li, Y., Li, Y., Li, D., Luo, Y., Wu, H., *et al.* From ultrafast to ultraslow: Charge-carrier dynamics of perovskite solar cells. *Joule* 2018, **2**(5)**:** 879-901.

18. Sum, T.C., Mathews, N., Xing, G., Lim, S.S., Chong, W.K., Giovanni, D., *et al.* Spectral features and charge dynamics of lead halideperovskites: Origins and interpretations. *Acc. Chem. Res.* 2016, **49**(2)**:** 294-302.

19. Yang, Y., Ostrowski, D.P., France, R.M., Zhu, K., van de Lagemaat, J., Luther, J.M., *et al.* Observation of a hot-phonon bottleneck in lead-iodide perovskites. *Nat. Photonics* 2015, **10**(1)**:** 53-59.

20. Fu, M., Tamarat, P., Trebbia, J.B., Bodnarchuk, M.I., Kovalenko, M.V., Even, J., *et al.* Unraveling exciton-phonon coupling in individual $FAPbI_3$ nanocrystals emitting near-infrared single photons. *Nat. Commun.* 2018, **9**(1)**:** 3318.

21. Manser, J.S., Kamat, P.V. Band filling with free charge carriers in organometal halide perovskites. *Nat. Photonics* 2014, **8**(9)**:** 737-743.

22. Dai, L., Deng, Z., Auras, F., Goodwin, H., Zhang, Z., Walmsley, J.C., *et al.* Slow carrier relaxation in tin-based perovskite nanocrystals. *Nat. Photonics* 2021.

23. Li, H., Hu, G., Li, B.-H., Zeng, W., Zhang, J., Wang, X., *et al.* Ultrahigh sensitive transient absorption spectrometer. *Rev. Sci. Instrum.* 2021, **92**(5)**:** 053002.

24. Lee, J.-W., Kim, D.-H., Kim, H.-S., Seo, S.-W., Cho, S.M., Park, N.-G. Formamidinium and Cesium Hybridization for Photo- and Moisture-Stable Perovskite Solar Cell. *Adv. Energy Mater.* 2015, **5**(20)**:** 1501310.

25. Herz, L.M. Charge-carrier dynamics in organic-inorganic metal halide perovskites. *Annu. Rev. Phys. Chem.* 2016, **67:** 65-89.

26. Yamada, Y., Nakamura, T., Endo, M., Wakamiya, A., Kanemitsu, Y. Photocarrier recombination dynamics in perovskite $CH_3NH_3PbI_3$ for solar cell applications. *J. Am. Chem. Soc.* 2014, **136**(33)**:** 11610-11613.

27. Sun, J., Yang, Y., Khan, J.I., Alarousu, E., Guo, Z., Zhang, X.*, et al.* Ultrafast carrier trapping of a metal-foped titanium dioxide semiconductor revealed by femtosecond transient absorption spectroscopy. *ACS Appl. Mater. Interfaces* 2014, **6**(13)**:** 10022-10027.

28. Righetto, M., Lim, S.S., Giovanni, D., Lim, J.W.M., Zhang, Q., Ramesh, S.*, et al.* Hot carriers perspective on the nature of traps in perovskites. *Nat. Commun.* 2020, **11**(1)**:** 2712.

29. Carpene, E., Mancini, E., Dallera, C., Schwen, D., Ronning, C., De Silvestri, S. Ultrafast carrier dynamics in tetrahedral amorphous carbon: carrier trapping versus electron–hole recombination. *New J. Phys.* 2007, **9**(11)**:** 404-404.

30. Wang, H., Zhang, C., Rana, F. Ultrafast dynamics of defect-assisted electron–hole recombination in monolayer MoS_2. *Nano Lett.* 2015, **15**(1)**:** 339-345.

31. Luo, D., Su, R., Zhang, W., Gong, Q., Zhu, R. Minimizing non-radiative recombination losses in perovskite solar cells. *Nat. Rev. Mater.* 2020, **5**(1)**:** 44-60.

32. Ball, J.M., Petrozza, A. Defects in perovskite-halides and their effects in solar cells. *Nat. Energy* 2016, **1**(11)**:** 16149.

33. Leijtens, T., Hoke, E.T., Grancini, G., Slotcavage, D.J., Eperon, G.E., Ball, J.M.*, et al.* Mapping electric field-induced switchable poling and structural degradation in hybrid lead halide perovskite thin films. *Adv. Energy Mater.* 2015, **5**(20)**:** 1500962.

34. Ni, Z., Bao, C., Liu, Y., Jiang, Q., Wu, W.-Q., Chen, S.*, et al.* Resolving spatial and energetic distributions of trap states in metal halide perovskite solar cells. *Science* 2020, **367**(6484)**:** 1352-1358.

35. Son, D.-Y., Lee, J.-W., Choi, Y.J., Jang, I.-H., Lee, S., Yoo, P.J.*, et al.* Self-formed grain boundary healing layer for highly efficient $CH_3NH_3PbI_3$ perovskite solar cells. *Nat. Energy* 2016, **1**(7)**:** 16081.

36. Niu, T., Lu, J., Munir, R., Li, J., Barrit, D., Zhang, X.*, et al.* Stable high-performance perovskite solar cells via grain boundary passivation. *Adv. Mater.* 2018, **30**(16)**:** 1706576.

37. Yoo, J.J., Seo, G., Chua, M.R., Park, T.G., Lu, Y., Rotermund, F.*, et al.* Efficient perovskite solar cells via improved carrier management. *Nature* 2021, **590**(7847).

38. Yang, S., Chen, S., Mosconi, E., Fang, Y., Xiao, X., Wang, C.*, et al.* Stabilizing halide perovskite

surfaces for solar cell operation with wide-bandgap lead oxysalts. *Science* 2019, **365**(6452)**:** 473-+.

39. Zheng, X., Chen, B., Dai, J., Fang, Y., Bai, Y., Lin, Y*., et al.* Defect passivation in hybrid perovskite solar cells using quaternary ammonium halide anions and cations. *Nat. Energy* 2017, **2**(7)**:** 17102.

40. Fu, L., Li, H., Wang, L., Yin, R., Li, B., Yin, L. Defect passivation strategies in perovskites for an enhanced photovoltaic performance. *Energy Environ. Sci.* 2020, **13**(11)**:** 4017-4056.

41. Ran, C., Xu, J., Gao, W., Huang, C., Dou, S. Defects in metal triiodide perovskite materials towards high-performance solar cells: origin, impact, characterization, and engineering. *Chem. Soc. Rev.* 2018, **47**(12)**:** 4581-4610.

42. Musiienko, A., Moravec, P., Grill, R., Praus, P., Vasylchenko, I., Pekarek, J*., et al.* Deep levels, charge transport and mixed conductivity in organometallic halide perovskites. *Energy Environ. Sci.* 2019, **12**(4)**:** 1413-1425.

43. Hoke, E.T., Slotcavage, D.J., Dohner, E.R., Bowring, A.R., Karunadasa, H.I., McGehee, M.D. Reversible photo-induced trap formation in mixed-halide hybrid perovskites for photovoltaics. *Chem. Sci.* 2015, **6**(1)**:** 613-617.

44. Hentz, O., Zhao, Z., Gradečak, S. Impacts of ion segregation on local optical properties in mixed halide perovskite films. *Nano Lett.* 2016, **16**(2)**:** 1485-1490.

45. Zhao, J.H., Schlesinger, T.E., Milnes, A.G. Determination of carrier capture cross sections of traps by deep level transient spectroscopy of semiconductors. *J. Appl. Phys.* 1987, **62**(7)**:** 2865-2870.

46. Shockley, W., Queisser, H.J. Detailed balance limit of efficiency of p-n junction solar cells. *J. Appl. Phys.* 1961, **32**(3)**:** 510-519.

47. Rühle, S. Tabulated values of the Shockley–Queisser limit for single junction solar cells. *Sol. Energy* 2016, **130:** 139-147.

48. Hirst, L.C., Ekins-Daukes, N.J. Fundamental losses in solar cells. *Prog. Photovolt: Res. Appl.* 2011, **19**(3)**:** 286-293.

49. Dar, M.I., Arora, N., Gao, P., Ahmad, S., Grätzel, M., Nazeeruddin, M.K. Investigation regarding the role of chloride in organic–inorganic halide perovskites obtained from chloride containing precursors. *Nano Lett.* 2014, **14**(12)**:** 6991-6996.

50. Williams, S.T., Zuo, F., Chueh, C.-C., Liao, C.-Y., Liang, P.-W., Jen, A.K.Y. Role of chloride in the morphological evolution of organo-lead halide perovskite thin films. *ACS Nano* 2014, **8**(10)**:**

10640-10654.

Acknowledgements

This work was supported by Ministry of Science and Technology of China (2018YFA0208700, 2019YFE0120000); Dalian Institute of Chemical Physics, Chinese Academy of Sciences (I202003); National Natural Science Foundation of China (22073097, 21688102); Chinese Academy of Sciences (YSBR-007, XDB17000000); Science and Technology Program of Sichuan Province (2021YFG0102, 2019YFG0513, and 2019ZDZX0015)

Author contributions

B.L., X.Y. and Z.R. conceived and designed experiments. B.L., H.L., W.Z., J.W. and Z.R. carried the transient absorption measurements. Z.X. and J.Z. prepared the perovskite samples and performed characterizations. B.L., H.L., C.Z., J.Z. and Z.R. analyzed the data. B.L., J.Z. X.Y. and Z.R. wrote the manuscript with input from all authors.

Additional information

Supplementary information is available in the online version of the paper. Reprints and permissions information is available online at www.nature.com/reprints. Correspondence and requests for materials should be addressed to Z.R.

Competing financial interests

The authors declare no competing financial interests.

Supplementary Files

This is a list of supplementary files associated with this preprint. Click to download.

- 20211223PerovskiteTALinearSINP.pdf